J Mol Model (2009) 15:913–922
DOI 10.1007/s00894-008-0445-2

ORIGINAL PAPER

Molecular modeling and dynamics studies of purine nucleoside phosphorylase from *Bacteroides fragilis*

Ivani Pauli · Luis Fernando Saraiva Macedo Timmers · Rafael Andrade Caceres · Luiz Augusto Basso · Diógenes Santiago Santos · Walter Filgueira de Azevedo Jr.

Received: 18 September 2008 / Accepted: 8 December 2008 / Published online: 27 January 2009

Abstract Purine nucleoside phosphorylase (PNP) catalyzes the reversible phosphorolysis of *N*-ribosidic bonds of purine nucleosides and deoxynucleosides, except adenosine, to generate ribose 1-phosphate and the purine base. This work describes for the first time a structural model of PNP from *Bacteroides fragilis* (*Bf*). We modeled the complexes of *Bf*PNP with six different ligands in order to determine the structural basis for specificity of these ligands against *Bf*PNP. Comparative analysis of the model of *Bf*PNP and the structure of *Hs*PNP allowed identification of structural features responsible for differences in the computationally determined ligand affinities. The molecular dynamics (MD) simulation was assessed to evaluate the overall stability of the *Bf*PNP model. The superposition of the final onto the initial minimized structure shows that there are no major conformational changes from the initial model, which is consistent with the relatively low root mean square deviation (RMSD). The results indicate that the structure of the model was stable during MD, and does not exhibit loosely structured loop regions or domain terminals.

Keywords *Bacteroides fragilis* · Bioinformatics · Drug-design · Molecular dynamics · Molecular modeling

I. Pauli · L. F. S. Macedo Timmers · R. Andrade Caceres · W. Filgueira de Azevedo Jr. (✉)
Laboratório de Bioquímica Estrutural, Faculdade de Biociências, Pontifícia Universidade Católica do Rio Grande do Sul, Porto Alegre, RS, Brazil
e-mail: walter@azevedolab.net
url: http://azevedolab.net

R. Andrade Caceres · L. Augusto Basso · D. Santiago Santos · W. Filgueira de Azevedo Jr.
Programa de Pós-Graduação em Medicina e Ciências da Saúde, Pontifícia Universidade Católica do Rio Grande do Sul, Porto Alegre, RS, Brazil

L. Augusto Basso · D. Santiago Santos
Instituto de Pesquisas Biomédicas, Centro de Pesquisas em Biologia Molecular e Funcional, Pontifícia Universidade Católica do Rio Grande do Sul, Porto Alegre, RS, Brazil

Introduction

Species of the genus *Bacteroides* are important constituents of both human and animal intestinal microbiota, comprising approximately 30% of the total cultured microorganisms from feces [1]. *Bacteroides fragilis* is considered the most virulent species in the genus *Bacteroides* due to its virulence factors and its predominance in monomicrobial and mixed infections of the brain and lung, intra-abdominal and intrapelvic abscess, peritonitis and sepsis [2]. Some strains of *B. fragilis* (ETBF) produce an enterotoxin that causes diarrhea in humans [3, 4]. This extracellular toxin has been characterized as a heat-labile zinc-metalloprotease of approximately 20 kDa and is a member of the metzincin superfamily [5]. Members of the *B. fragilis* group have been studied because of their pathogenic potential and because of their unusual multiple resistance to several antibiotics [6, 7], which can be transferred within and between species, including Gram-negative facultative anaerobic bacteria, such as *Escherichia coli* [8]. Taking these facts into account, it is necessary to discover new antibacterial drugs, using protein targets to guide virtual screening initiatives.

Several studies on purine nucleoside phosphorylase (PNP) have suggested this enzyme as a target for the development of antibacterial drugs [9–12]. PNP catalyzes the cleavage of *N*-ribosidic bonds of purine ribonucleosides

and 2-deoxyribonucleosides in the presence of inorganic orthophosphate as a second substrate. This reaction generates the purine base and ribose(deoxyribose)-1-phosphate [13]. PNP is specific for purine nucleosides in the β-configuration and cleaves the glycosidic bond with inversion of configuration to produce α-ribose-1-phosphate [14]. PNP is a ubiquitous enzyme of purine metabolism that functions in salvage pathways, including those of Apicomplexan parasites [15]. PNP is classified as belonging to class I nucleoside phosphorylases (NP-I) [16]. Drugs that inhibit human PNP activity have the potential of being utilized as modulators of the immune system, to treat leukemia, autoimmune diseases, and rejection in organ transplantation [9, 17]. PNP has been submitted to intensive studies focused on the identification of new inhibitors, most of them related to human PNP.

In the present work, we modeled the structure of PNP from *B. fragilis* (*Bf*PNP) using a molecular modeling approach. We analyzed three binding sites present in the structures of human PNP and *Bf*PNP. The analysis was carried out with different ligands in order to identify the structural basis for the specificity of different ligands against PNPs. Furthermore, an understanding of the rules governing the specificity of different ligands against PNP could be used to help design more specific inhibitors and, in the case of *Bf*PNP, help in the development of a new drug against *B. fragilis*.

Materials and methods

Molecular modeling

Homology modeling is usually the method of choice when there is a clear relationship of homology between the sequences of a target protein and at least one experimentally determined three-dimensional (3D) structure [18]. This computational technique is based on the assumption that the tertiary structures of two proteins will be similar if their sequences are related, and it is the approach most likely to give accurate results [19]. For modeling of *Bf*PNP complexed with acyclovir, guanine, 7-methyl-6-thio-guanosine, 3-deoxyguanosine, guanosine and inosine the following crystallographic structures were used as templates: 1PWY [20], 1V2H [21], 1YRY [22], 1V45, 1RFG [23] and 1RCT [24], respectively. The latter structures, which are all human PNPs solved by crystallography methods, were chosen by an advanced search of the Protein Data Bank (PDB), where the target sequence, in our case *Bf*PNP, was submitted to a blast/fasta alignment against the deposited data in the PDB. The search output is a list of the related sequences available in the PDB along with the percentage of identity. The high degree of primary sequence identity between *Bf*PNP (target) and human PNP (*Hs*PNP) (46%) indicates that these crystallographic structures are good models to be used as templates for the *Bf*PNP enzyme (target). An alignment of *Bf*PNP (target) and human PNP is shown in Fig. 1 [25]. The web server PARMODEL was used to model the binary complexes [26]. PARMODEL is a parallelized version of MODELLER [27]. The modeling procedure begins with alignment of the sequence to be modeled (target) with known related 3D structures (templates). This alignment is usually the input to the program, and the output is a 3D model of the target sequence containing all main-chain and side-chain non-hydrogen atoms [28]. A total of 1,000 models were generated for each binary complex, and the final models were selected based on an objective function of MODELLER [27]. All optimization process was performed on a Beowulf cluster with 16 nodes (BioComp, AMD Athlon XP 2100+, BioComp, Brazil).

Evaluation of binding affinity

Analysis of the interaction between a ligand and a protein target is still a scientific endeavor. The affinity and specificity between a ligand and its protein target depend on directional hydrogen bonds and ionic interactions, as well as on shape complementarity of the contact surfaces of

```
                10        20        30        40        50
        ....|....|....|....|....|....|....|....|....|....|
BfPNP   --MTLLEKINETRDFLQAKGVTAPEFGLILGSGLGELAEEIENPIVVDYA
HsPNP   ENGYTYEDYKNTAEWLLSHTKHRPQVAIICGSGLGGLTDKLTQAQIFDYS
              *. ::* ::* ::    *:..:* ***** *:::: :. :.**:

                60        70        80        90        100
....|....|....|....|....|....|....|....|....|....|
BfPNP   DIPNWGQSTVVGHAGKLVYGDLSGRKVLALQGRFHFYEGNTMEVVTFPVR
HsPNP   EIPNFPRSTVPGHAGRLVFGFLNGRACVMMQGRFHMYEGYPLWKVTFPVR
        :***: :*** ****:**:* *.**  : :*****:*** .:  ******

                110       120       130       140       150
        ....|....|....|....|....|....|....|....|....|....|
BfPNP   IMRALACHSVLVTNAAGGIG--YGPGTLMLIKDHINMIG---TNPLIGEN
HsPNP   VFHLLGVDTLVVTNAAGGLNPKFEVGDIMLIRDHINLPGFSGQNPLRGPN
        ::: *. .::*******:.  :  * :***:****: *    *** * *

                160       170       180       190       200
        ....|....|....|....|....|....|....|....|....|....|
BfPNP   LEEFGPRFPDMSDAYTATYRQKAHQIAEKQ--NIKLEEGVYLGVSGPTYE
HsPNP   DERFGDRFPAMSDAYDRTMRQRALSTWKQMGEQRELQEGTYVMVAGPSFE
         *.** *** *****  * **:* .  ::   : :*:**.*: *:**::*

                210       220       230       240       250
        ....|....|....|....|....|....|....|....|....|....|
BfPNP   TPAEIRAFQTMGAQAVGMSTVPEVIVAAHSGLKVLGISAITN-FAAGFQS
HsPNP   TVAECRVLQKLGADAVGMSTVPEVIVARHCGLRVFGFSLITNKVIMDYES
        * ** *.:*.:**:************** *.**:*:*:* *** .  .::*

                260       270       280
        ....|....|....|....|....|...
BfPNP   --ELNHEEVVEVTQRIKEDFKGLVKSLVAEL-------
HsPNP   LEKANHEEVLAAGKQAAQKLEQFVSILMASIPLPDKAS
  : *****: . ::  :.:: :*. *:*.:
```

Fig. 1 Sequence alignment of human purine nucleoside phosphorylase (*HsPNP*) and PNP from *Bacteroides fragilis* (*BfPNP*). The alignment was performed using ClustalW and edited with BioEdit [23]. Asterisks Fully conserved positions, *colons* 'strong' group amino acids conserved, *periods* 'weaker' group amino acids conserved

Fig. 2 Structure of the *Bf*PNP. The structure (presented as a ribbon diagram) contains an eight-stranded mixed beta-sheet and a five-stranded mixed beta-sheet, which join to form a distorted beta-barrel. The image was generated using Pymol [47]

both partners [29]. In addition, σ-hole concept has also played an important role in the analysis of intermolecular interaction [30, 31].

The program SCORE [32] was used to evaluate the binding affinity of ligands against *Hs*PNP and *Bf*PNP. According to this method, the binding affinity of the ligand can be split up to give the contribution of individual atoms. Each ligand atom obtains a score, called the atomic binding score, indicating its role in the binding process. The program reads the structure, assigns atom types and parameters, performs the calculation, and gives the dissociation constant of the given protein–ligand complex.

The computational results are fed into a text file in which the detailed information of each ligand atom, including the atomic binding score, is tabulated. These data were then used to evaluate the correlation coefficient between the affinities against both PNPs to verify possible similarities in the structural basis for specificity against these enzymes.

Analysis of the models

The overall stereochemical quality of the final models for each enzyme of *Bf*PNP was assessed by the program PROCHECK [33]. The objective function was supplied by the program MODELLER [26]. The atomic models were superposed using the program LSQKAB from CCP4 [34] and the intermolecular hydrogen bonds were assessed by the program LIGPLOT [35].

Molecular dynamics simulations

Molecular dynamics (MD) simulations were performed with the GROMACS [36] package using the Gromos 96.1

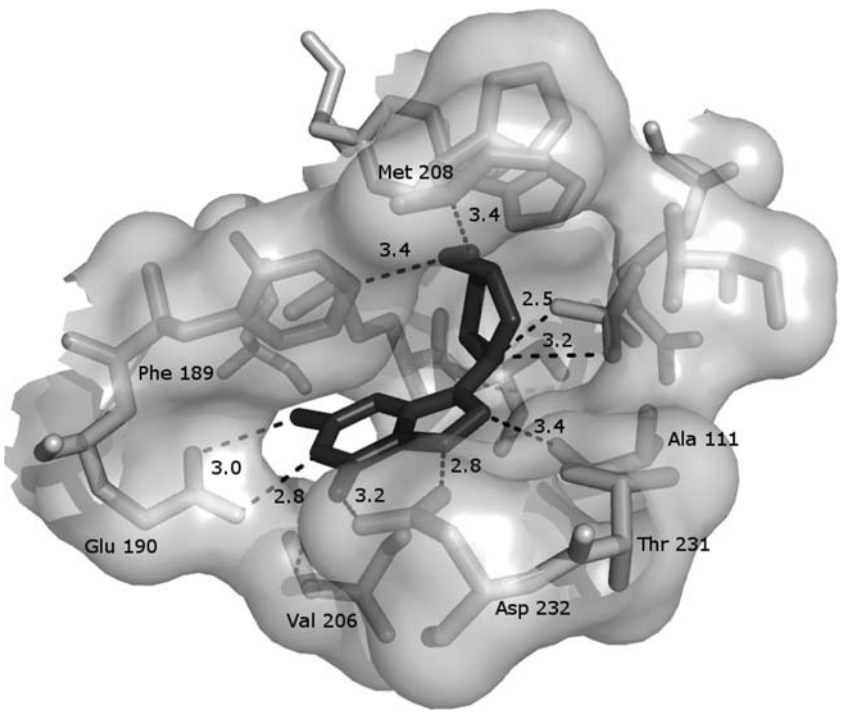

Fig. 3 Representation of the active site of *Bf*PNP with 3-deoxyguanosine. *Light gray* *Bf*PNP residues, *dark gray* inhibitor (3-deoxyguanosine) residues. The image was generated using Pymol [47]

Fig. 4 Superposition of the *Hs*PNP-acyclovir complex (*light gray*) on the *Bf*PNP-acyclovir complex (*dark gray*). The image was generated using Pymol [47]

(53A6) force field [37]. The Acyclovir (ACY) topology was generated with the PRODRG program [38].

Accurate force fields are essential for reproducing the conformational and dynamic behavior of condensed-phase systems. The Gromos 96.1 force fields are well parameterized for proteins, but the parameters for small molecules are still limited for simulations of more complicated biological systems. So, to generate the atomic charges in the ACY molecule we used GAMESS [39], which were submitted to single-point ab initio calculations at RHF 6-31G* level (E) in order to obtain Löwdin derived charges [40].

Manipulation of structures was performed with the program Swiss-PDBViewer v3.7 [41]. The first system comprised apoenzyme *Bf*PNP (system A) and the second, *Bf*PNP enzyme, three sulfate ions and ACY ligand (system B).

Simulations of the two systems were performed in time periods of 3 ns. In both systems, Na^+ was added as counter ions (7 Na^+ ions in system A and 11 in system B) using the *Genion* Program of the GROMACS simulation suite to neutralize the negative charge density of the systems.

Each structure was placed in the center of a truncated dodecahedric box filled with simple point charge (SPC) water molecules [42], containing 11,685 water molecules for system A and 10,481 for system B. The initial simulation cell dimensions were 47.8 Å × 48.6 Å × 51.2 Å for system A and 49.0 Å × 42.4 Å × 52.0 Å for system B, and had the protein solvated with a layer of water molecules of at least 10 Å in all directions in both systems. The cell dimensions used for these simulations are based on the protein volume, which ensure a minimum distance (in this case 10 Å) between the solute and the face of the box.

During the simulations, bond lengths within the proteins were constrained using the LINCS algorithm [43]. The SETTLE algorithm was used to constrain the geometry of water molecules [44]. In the MD protocol, all hydrogen atoms, ions, and water molecules were first subjected to 1,000 steps of energy minimization by steepest descent, followed by 500 steps of conjugate gradient to remove close van der Waals contacts.

The systems were then submitted to a short MD with position restraints for a period of 20 ps, and afterwards a full MD without restraints was performed. The temperature of the system was then increased from 50 K to 300 K in five steps (50 K–100 K, 100 K–150 K, 150 K–200 K, 200 K–250 K, 250 K–300 K), and the velocities at each step were reassigned according to the Maxwell-Boltzmann

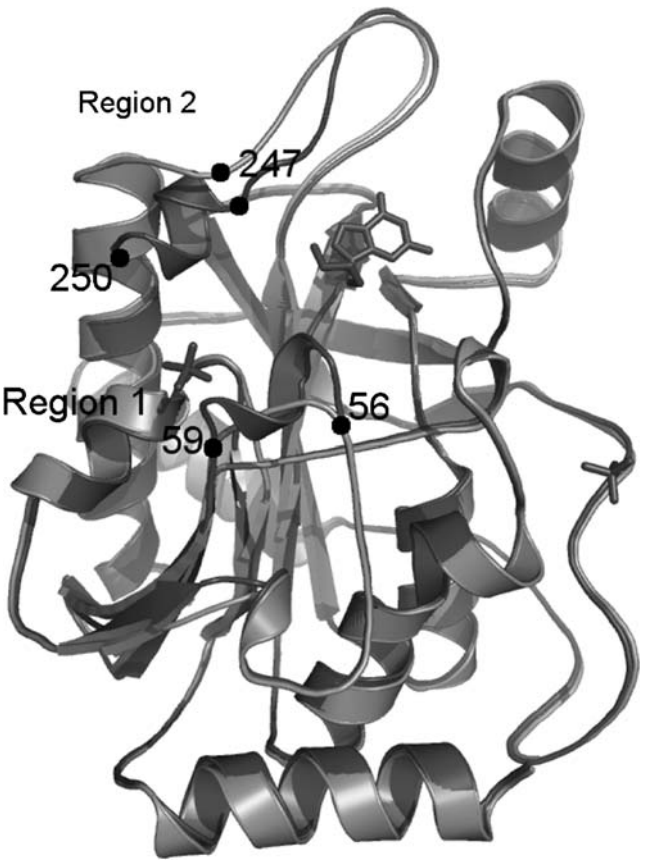

Fig. 5 Superimposition of *Bf*PNP apoenzyme (*light gray*) on the *Bf*PNP-acyclovir complex (*dark gray*). Regions 1 and 2 indicate the conformational changes due ligand binding. The image was generated using Pymol [47]

Table 1 Intermolecular contacts of human purine nucleoside phosphorylase (HsPNP) with ligands

Residues/ligands	Guanine	Guanosine	3-Deoxyguanosine	7-Methyl-6-thio-guanosine	Acyclovir	Inosine
Glu201	OE2-N1 → 2.4 Å	OE2-N1 → 2.4 Å	OE2-N1 → 2.7 Å	OE2-N1 → 2.9 Å	OE2-N1 → 3.0 Å	OE2-O6 → 3.3 Å
	OE2-N2 → 2.8 Å	OE1-N2 → 2.6 Å	OE1-N2 → 2.7 Å	OE1-N2 → 2.7 Å	OE1-N2 → 2.5 Å	
Asn243	ND2-O6 → 2.8 Å	ND2-N7 → 3.1 Å	ND2-O6 → 3.3 Å	–	ND2-N7 → 2.9 Å	ND2-O6 → 2.8 Å
		ND2-O6 → 2.8 Å	OD1-N7 → 2.7 Å		ND2-O6 → 2.6 Å	ND2-N7 → 3.3 Å
His257	–	–	ND1-O5′ → 2.8 Å	–	–	ND1-O5* → 2.9 Å
Tyr88	–	OH-O3* → 3.2 Å	–	OH-O3* → 2.7 Å	–	OH-O3* → 3.0 Å
Ala116	–	O-O2* → 3.1 Å	–	–	–	O-O2* → 3.4 Å
Met219	–	N-O2* → 3.0 Å	N-O2′ → 3.0 Å	N-O2* → 3.0 Å	–	N-O2* → 3.0 Å

distribution at that temperature and equilibrated for 10 ps except for the final part of the thermalization phase, where we used a period of 40 ps.

Energy minimization and MD were carried out under periodic boundary conditions. The simulation was computed in the NPT ensemble at 300 K with Berendsen temperature coupling and a constant pressure of 1 atmosphere with isotropic molecule-based scaling [45]. The LINCS algorithm, with a 10^{-5} Å tolerance, was applied to fix all bonds containing a hydrogen atom, allowing the use of a time step of 2.0 fs in the integration of the equations of motion. No extra restraints were applied after the equilibration phase.

Electrostatic interactions between non-ligand atoms were evaluated by the particle-mesh Ewald method [46] with a charge grid spacing of ~1.0 Å; the charge grid was interpolated on a cubic grid with the direct sum tolerance set to 1.0×10^{-5}. The Lennard-Jones interactions were evaluated using a 9.0 Å atom-based cutoff [47].

All analysis were performed on the ensemble of system configurations extracted at 0.5-ps time intervals from the simulation, and MD trajectory collection was initiated after 1 ns of dynamics to guarantee a completely equilibrated evolution. The MD simulation and results analysis were performed on a personal computer with an Intel Core 2 Duo E6300—1.86 GHz processor and 4 GB RAM.

The convergence of the different simulations were analyzed in terms of the secondary structure, root mean-square deviation (RMSD) from the initial models structures, and root mean-square fluctuation (RMSF) to estimate the B-factor. For B-factor calculation, RMSFs were calculated relative to the last 2 ns averaged backbone structures, and all coordinate frames from the trajectories were first superimposed on the initial conformation to remove any effect of overall translation and rotation. Atomic isotropic B-factors were calculated from trajectories using the equation

$$\mathrm{B-factor_i} = \left(8\pi^2/3\right)\left(\left\langle \mathrm{r_i^2}\right\rangle - \left\langle \mathrm{r_i}\right\rangle^2\right),$$

where $\left(\left\langle \mathrm{r_i^2}\right\rangle - \left\langle \mathrm{r_i}\right\rangle^2\right)$ is the mean-square positional fluctuation of atom *i* [48, 49].

Results and discussion

Quality of the models

No crystallographic structure for *Bf*PNP is available; however, the similarity between *Bf*PNP and *Hs*PNP sequences makes the *Hs*PNP structure a reasonable template for modeling of *Bf*PNP. Furthermore, there are several binary complexes between human PNP and different ligands, which make available templates to model binary complexes of *Bf*PNP against these ligands.

The atomic coordinates of crystallographic structures of the templates were used as basic models for modeling of *Bf*PNP. The atomic coordinates of all water molecules were removed from the templates. Analysis of the Ramachandran diagram φ–ψ plots for the templates (*Hs*PNP) was used to compare the overall stereochemical quality of the *Bf*PNP structures against those of templates solved by biocrystallography.

The homology models present over 90% of the residues in the most favorable regions. The RMSD values for

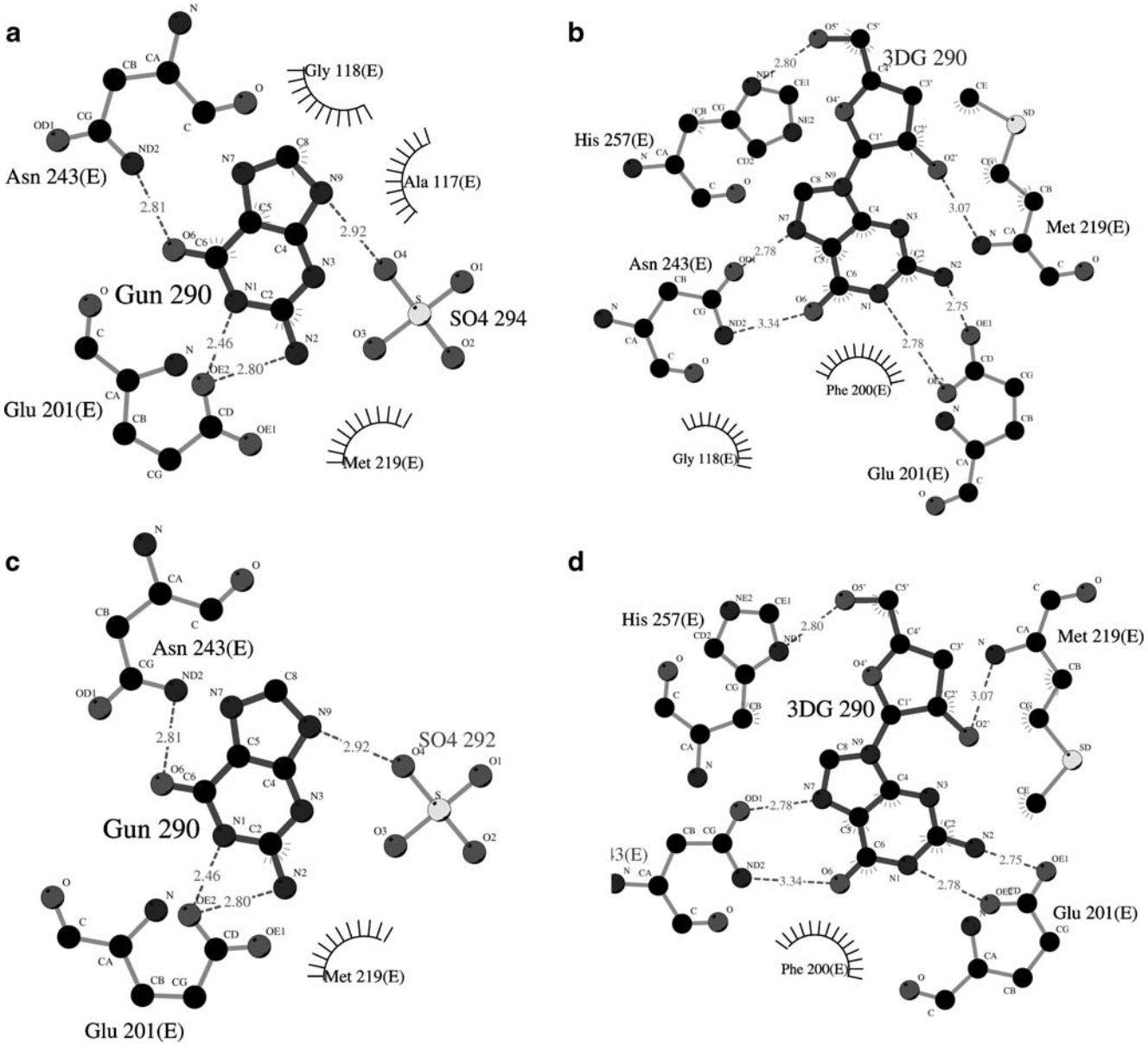

Fig. 6 a–d Intermolecular contacts. **a** *Bf*PNP with guanine, **b** *Hs*PNP with guanine, **c** *Bf*PNP with 3-deoxyguanosine, **d** *Hs*PNP with 3-deoxyguanosine. The images were generated using Ligplot [33]

superposition of the active binding sites and proteins for human PNP and *Bf*PNP range from 0.1 Å to 1.4 Å and 0.4 Å to 0.5 Å, respectively.

Overall description

The structural model of *Bf*PNP indicates that it belongs to the class α/β, consisting of a mixed β-sheet and α-helices; the structure exhibits a distorted beta-barrel surrounded by alpha-helices.

The structure contains an eight-stranded mixed beta-sheet, and a five-stranded mixed beta-sheet, which join to form a distorted beta-barrel. The residues making up the eight-stranded sheet are 22–26, 41–43, 62–68, 71–77, 104–115, 123–131, 177–184, and 223–231. The five-stranded sheet consists of residues 110–115, 123–128, 177–181, 204–207, and 226–231.

Seven alpha-helices surround the beta-sheet structure. The alpha-helices are composed of residues 3–15, 31–35, 88–101, 159–172, 192–201, 211–220, and 249–268.

Figure 2 [50] show schematic drawings of the *Bf*PNP structure (monomer). Figure 3 shows a representation of the active-site of *Bf*PNP.

Table 2 Intermolecular contacts of *Bacteroides fragilis* PNP (*Bf*PNP) with ligands

Residue/ligand	Guanine	Guanosine	3-Deoxyguanosine	7-Methyl-6-thio-guanosine	Acyclovir	Inosine
Asn232	OD1-N7 → 2.6 Å	ND2-O6 → 2.9 Å	OD1-N7 → 2.8 Å		ND2-N7 → 2.8 Å	ND2-O6 → 2.8 Å
	ND2-O6 → 2.7 Å	ND2-N7 → 3.1 Å	ND2-O6 → 3.3 Å	–	ND2-O6 → 2.7 Å	ND2-N7 → 3.2 Å
		OD1-N7 → 2.7 Å				OD1-N7 → 2.6 Å
Glu191	OE2-N1 → 2.6 Å	OE2-N1 → 2.6 Å	OE2-N1 → 2.8 Å	OE2-N1 → 2.9 Å	OE2-N1 → 2.9 Å	OE2-N1 → 2.6 Å
	OE2-N2 → 2.8 Å	OE1-N2 → 2.9 Å	OE1-N2 → 2.9 Å	OE1-N2 → 2.8 Å	OE1-N2 → 2.7 Å	
Tyr190	–	–	OH-O5′→ 2.4 Å	OH-O5* → 2.6 Å	–	–
Met209	–	N-O2* → 3.1 Å	N-O2′ → 3.0 Å	N-O2* → 3.1 Å	–	N-O2* → 3.1 Å
Tyr85	–	OH-O3* → 3.2 Å	–	OH-O3* → 2.6 Å	–	OH-O3* → 3.0 Å
His244	–	–	ND1-O5′ → 2.8 Å	–	–	ND1-O5* → 2.9 Å

The binary complexes were modeled with six ligands (guanine, guanosine, 3-deoxyguanosine, 7-methyl-6-thio-guanosine, inosine and acyclovir). The identity between human *Hs*PNP and *Bf*PNP (~46%) classifies *Bf*PNP as a member of the nucleosides phosphorylase (NP)-I group, more specifically as low-molecular-mass (low-mm) homo-trimers, with M_r~ 80–100 kDa, specific for catalysis of 6-oxopurines and their nucleosides.

*Bf*PNP (EC 2.4.2.1) consists of 269 amino acids, and has a molecular weight of 29,091.3 Da and a theoretical pI of 5.12. *Hs*PNP consists of 288 amino acids, and has a molecular weight of 32,016.7 Da and a theoretical pI of 6.50.

Analysis of the structure of both PNPs indicates that, despite conservation of the ribose-binding site, three mutations are observed in other sites: one in the purine-binding site, one in the first phosphate-binding site, and one in the second phosphate-binding site. Asn243, Ser33 and Gln144 in human PNP [49] are replaced by Asp232, Thr28 and Glu136, respectively, in *Bf*PNP.

Furthermore, superposition of the *Bf*PNP structure onto that of *Hs*PNP (Fig. 4) indicates that a small region involving residues 247–250 presents a small helical region not observed in the *Hs*PNP structure (residues 260–263). The sequence alignment indicates that this region is not conserved (see Fig. 1). Analysis of the propensity to form helix using the Chow and Fasman scale [51] and PSIPRED (Protein Structure Prediction Server) [52] was not conclusive, indicating only a slightly higher propensity to form turns in the *Hs*PNP sequence.

Differences between the apoenzyme and the binary complexes

In order to evaluate possible differences in the *Bf*PNP structure due to ligand binding, we superimposed the structure of the apoenzyme, modeled using *Hs*PNP as template (PDB access code: 1M73) [53], on the six binary complexes. The RMSD for C-alpha superposition range from 0.7 to 1.0 Å. In all binary complexes, the highest differences are observed in two regions, region 1 from 56 to 59, and region 2 from 247 to 250. Region 2 exhibits large conformation differences in all six binary complexes, and region 1 exhibits the highest differences only for the *Bf*PNP-acyclovir complex. Taken together, these findings indicate the flexibility of these two regions, which allows different ligands to bind to the PNP active site. The highest values (1.0 Å) are observed for the PNP-3-deoxyguanosine complex. This region undergoes a conformational change due to ligand binding. Figure 5 shows the superimposition of the *Bf*PNP apoenzyme on the *Bf*PNP-acyclovir complex—both regions can be seen clearly.

Interactions with ligands

There are a plethora of methods to evaluate protein-ligand interactions [54–63]. The binding affinity of protein–ligand complexes for human PNP and *Bf*PNP were calculated with the program SCORE and the results are shown in Table 1. The correlation coefficient between the affinity constants for *Hs*PNP and *Bf*PNP is 0.2. The affinity of the six ligands

Table 3 pKd values for *Hs*PNP and *Bf*PNP. The results were generated using SCORE [32]

PNP/ligand	Acyclovir	Guanine	Guanosine	3-Deoxyguanosine	7-Methyl-6-thio-guanosine	Inosine
*Hs*PNP	4.04	5.22	4.92	5.76	3.44	4.39
*Bf*PNP	3.11	4.18	3.88	4.52	4.12	4.17

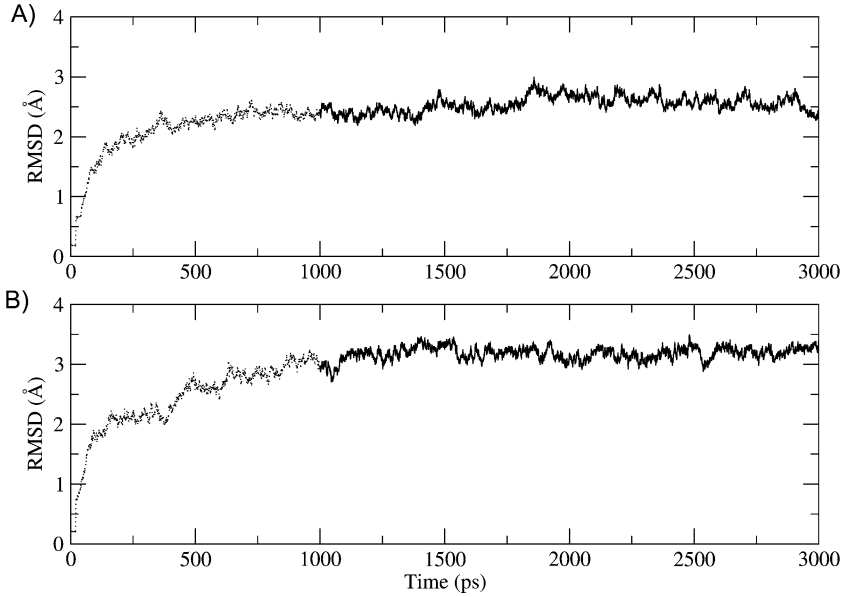

Fig. 7 a, b Graphical representation of root-mean-square deviation (RMSD) of all Cα from the starting model structure as a function of time. **a** RMSD of apoenzyme BfPNP, **b** RMSD of *Bf*PNP-ACY complex. *Dashed line* Equilibration phase, *solid line* last 2 ns of calculation

for *Hs*PNP and *Bf*PNP indicates strongly that there is no correlation between the affinities for both PNPs. Figure 6 shows the intermolecular contacts between enzyme and ligands for the complexes with highest affinity constants. The ligands 3-deoxyguanosine and guanine presents the highest affinities for both PNPs. Tables 2 and 3 show the intermolecular hydrogen bonds for all complexes studied in this article. We can see clearly that the intermolecular hydrogen bonds involving Glu201/Glu190 and Asn243/Asp232 are conserved in all complexes.

MD simulations

To obtain an estimate of the MD trajectory quality convergence, the backbone RMSD from the starting model structures were calculated (Fig. 7). After a rapid increase during the first 250 ps, the protein backbone RMSD average and standard deviation over the last 2 ns of the system A and B trajectories was 2.4±0.1 Å and 3.2±0.1 Å, respectively. A plateau of RMSDs for both systems was achieved within 750 ps of unrestrained simulation, suggesting that 2.9 ns unrestrained simulation was sufficient for stabilizing the fully relaxed models.

The superimposition of the average structure of system A with the initial model (Fig. 8) showed no major conformational changes from the initial model, which is consistent with the relatively low RMSD value. The protein flexibility was assessed by the B-factor from the MD trajectory and reflects the flexibility of each atomic residue in the molecule. In a typical B-factor pattern, low B-factor values indicate highly-structured regions while high values indicate loosely structured loop regions or domain termini [64].

Loop L1–L4 in Fig. 9 shows the four high B-factor regions. It is obvious that the major backbone fluctuations occur in the loop region and in the region surrounding the beta-alpha-beta fold, whereas regions with the low B-factor correspond exclusively to the rigid beta-alpha-beta fold. These facts indicate the stability of our model structures. The large mobility of loops L1–L4—mainly loop L4 composed of THR231–HIS244 (Fig. 9)—is consistent with the requirement for this region to undergo conformational

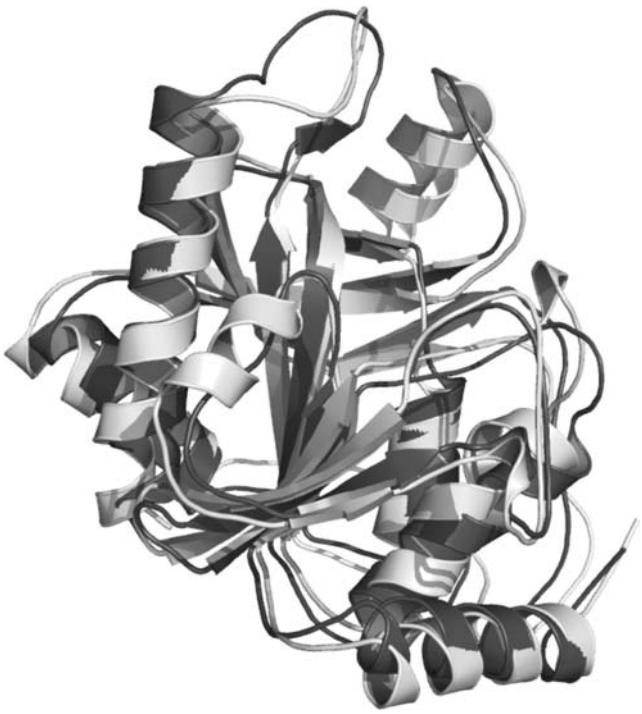

Fig. 8 Superimposition of the average of the final 2,000 snapshots, with the initial minimized structure of apoenzyme BfPNP. The structures are presented as a ribbon diagram. *Dark gray* Average structure, *light gray* initial structure

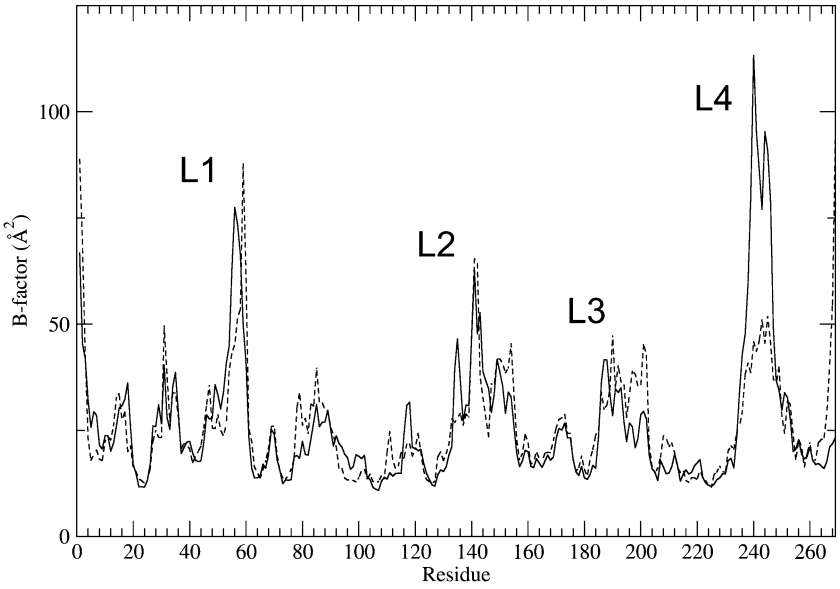

Fig. 9 Backbone residue-based B-factors calculated over the final 2 ns time window for BfPNP (*solid line*) and the BfPNP-acyclovir (ACY) complex (*dashed line*). *L1–L4* Regions with high fluctuation in the simulation

changes upon substrate biding. In loop L4, the differences in behavior between system A and system B is evident, demonstrating that acyclovir induces major stability in this region, as the substrate binding loop and Loop 4 are involved in substrate entrance and exit.

Finally, from the superimposition of the backbone of the average final 2 ns structure and the initial structure of system B (Fig. 10), we observed that it does not change much, except in regions L4 and L3, where the backbone moves backwards slightly.

Fig. 10 Superimposition of the average of the last 2,000 snapshots with the initial minimized structure of the BfPNP-ACY complex. The structures are presented as a ribbon diagram with ACY in stick diagram format. *Dark gray* Average structure, *light grey* initial structure

Conclusions

Structural analysis of human PNP and BfPNP has revealed three mutations in the binding-pocket: one in the purine-binding site, one in the first phosphate-binding site and one in the second phosphate-binding site, which could explain the differences observed in the affinity constants for both PNPs. Furthermore, the computationally determined affinity constant of the inhibitor guanosine for *Bf*PNP and *Hs*PNP indicates strongly that this inhibitor has high affinity for *Bf*PNP, suggesting a possible new lead compound against *Bacteroides fragilis*. To better understand the inter-monomer dynamics within the enzyme, ideally a trimer *Bf*PNP MD simulation would be run; however, this would be expensive in terms of computing costs. The major goal of this study is to characterize the dynamic behavior of the enzyme and the mode of substrate binding, thus helping to design a selective inhibitor of PNP of *B. fragillis*. Therefore, simulation of the monomer rather than the trimer does not change the major conclusions of our study.

Acknowledgments This work was supported by grants from Conselho Nacional de Pesquisas (CNPq), Coordenação de Aperfeiçoamento de Pessoal de Nível Superior (CAPES) and Instituto Nacional de Ciência e Tecnologia (INCT-CNPq-MCT). W.F.A., D.S.S. and L.A.B. are senior researchers of CNPq (Conselho Nacional de Pesquisas, Brazil).

References

1. Myers LL, Shoop DS, Stackhouse LL, Newman FS, Flaherty RJ, Letson GW, Sack RB (1987) J Clin Microbiol 12:2330–2333
2. Duerden BI, Collee JG, Brown R, Deacon AG, Holbrook WP (1980) J Med Microbiol 13:231–245
3. Border M, Feirehammer BD, Shoop DS, Myers LL (1985) J Clin Microbiol 21:472–473
4. Almeida FS, Nakano V, Avila-Campos MJ (2007) FEMS Microbiol Lett 272:15–21
5. Wu S, Shin J, Zhang G, Cohen M, Franco A, Sears CL (1984) Infect Immun 74:5382–5390
6. Salyers AA (1984) Annu Rev Microbiol 38:293–313
7. Nakano V, Avila-Campos MJ (2004) Mem Inst Oswaldo Cruz 99:319–324
8. Gupta A, Vlamakis H, Shoemarker N, Salyers AA (2003) Appl Environ Microbiol 69:6455–6463
9. Silva RG, Nunes JES, Canduri F, Borges JC, Gava LM, Moreno FB, Basso LA, Santos DS (2007) Curr Drugs Target 8:413–422
10. Caceres RA, Saraiva Timmers LF, Dias R, Basso LA, Santos DS, de Azevedo WF Jr (2008) Bioorg Med Chem 16:4984–93
11. Canduri F, Fadel V, Dias MVB, Basso LA, Palma MS, Santos DS, De Azevedo WF Jr (2005) Biochem Biophys Res Commun 326:335–338
12. De Azevedo WF, Canduri F, Santos DM, Pereira JH, Dias MVB, Silva RG, Mendes MA, Basso LA, Palma MS, Santos DS (2003) Biochem Biophys Res Commun 309:917–922
13. Kalckar HM (1947) J Biol Chem 167:429–443
14. Canduri f, Fadel V, Basso LA, Palma MS, Santos DS, de Azevedo WF Jr (2005) Biochem Biophys Res Commun 327:646–649
15. Bzowska A, Kulikowska E, Shugar D (2000) Pharmacol Ther 88:349–425
16. Pugmire MJ, Ealick SE (2002) Biochem J 361:1–25
17. Timmers LFSM, Caceres RA, Vivan AL, Gava LM, Dias R, Ducati RG, Basso LA, Santos DS, de Azevedo WF Jr (2008) Arch Biochem Biophys 479:28–38. doi:10.1016/j.abb.2008.08.015
18. Pauli I, Caceres RA, de Azevedo WF Jr (2008) Bioorg Med Chem 16:8098–8108
19. Kroemer RT, Doughty SW, Robinson AJ, Richards WG (1996) Protein Eng 9:493–498
20. dos Santos DM, Canduri F, Pereira JH, Dias MVB, Silva RG, Mendes MA, Palma MS, Basso LA, de Azevedo WF, Santos DS (2003) Biochem Biophys Res Commun 308:553–559
21. de Azevedo WF, Canduri F, dos Santos MD, Pereira JH, Dias MVB, Silva RG, Mendes MA, Basso LA, Palma MS, Santos DS (2003) Biochem Biophys Res Commun 312:767–772
22. Silva RG, Pereira JH, Canduri F, de Azevedo WF Jr WF, Basso LA, Santos DS (2005) Arch Biochem Biophys 442:49–58
23. Canduri F, Silva RG, Dos Santos DS, Palma MS, Basso LA, Santos DS, de Azevedo WF (2005) Acta Crystallogr D 61:856–862
24. Canduri F, dos Santos DM, Silva RG, Mendes MA, Basso LA, Palma MS, de Azevedo WF Jr, Santos DS (2004) Biochem Biophys Res Comm 313:907–914
25. Hall TA (1999) Nucleic Acids Symp Ser 41:95–98
26. Uchoa HB, Jorge GE, Da Silveira NJF, Camera JC, Canduri F, de Azevedo WF (2004) Biochem Biophys Res Commun 325:1481–1486
27. Sali A, Blundell TL (1993) J Mol Biol 234:779–815
28. Canduri F, Uchoa HB, de Azevedo WF (2004) Biochem Biophys Res Commun 324:661–666
29. de Azevedo WF, Mueller-Dieckmann JH, Schulze-Gahmen U, Worland PJ, Sausville E, Kim SH (1996) Proc Natl Acad Sci USA 93:2735–2740
30. Politzer P, Murray JS, Lane P (2007) Int J Quant Chem 107:3046–3052
31. Murray S, Lane P, Clark T, Politzer P (2007) J Mol Mod 13:1033–1038
32. Wang R, Liu L, Lai L, Tang Y (1998) J Mol Mod 4:379–394
33. Laskowski RA, Macarthur MW, Moss DS, Thornton JM (1993) J Appl Crystallogr 26:283–291
34. Collaborative Computation Project, Number 4 (1994) Acta Crystallogr D 50:760–763
35. Wallace AC, Laskowski RA, Thornton JM (1995) Protein Eng 8:127–134
36. van der Spoel D, Lindahl E, Hess B, Groenhof G, Mark AE, Berendsen HJC (2005) J Comp Chem 26:1701–1718
37. Ooestenbrik C, Soares TA, van der Vegt NFA, van Gunsteren WF (2005) Eur Biophys J 34:273–284
38. van Aalten DMF, Bywater B, Findlay JBC, Hendlich M, Hooft RWW, Vriend GJ (1996) Comput Aided Mol Des 10:255–262
39. Schmidt MW, Baldridge KK, Boatz JA, Elbert ST, Gordon MS, Jensen JH, Koseki S, Matsunaga N, Nguyen KA, Su SJ, Windus TL, Dupuis M, Montgomery JAJ (1993) Comput Chem 14:1347–1363
40. Hofer TS, Randolf BR, Rode BM (2008) J Phys Chem B 48 (1):85–98
41. Guex N, Peitsch MC (1997) Electrophoresis 18:2714–2723
42. Berendsen HJC, Postma JPM, Van Gunsteren WF, Hermans J (1981) In: Pullman B (ed) Intermolecular forces. Reidel, Dordrecht
43. Hess B, Bekker H, Berendsen HJC, Fraaije JGEM (1997) J Comput Chem 18:1463
44. Miyamoto S, Kollman PA (1992) J Comput Chem 13:952
45. Chowdhuri S, Tan ML, Ichiye T (2006) J Chem Phys 125:144513
46. Darden T, York D, Pedersen LA (1993) J Chem Phys 98:10089–10092
47. De Souza ON, Ornstein RL (1999) J Biomol Struct Dyn 16:1205–1218
48. Hünenberger PH, Mark AE, Van Gunsteren WF (1995) J Mol Biol 252:492–503
49. Van Gunsteren WF, Mark AE (1998) J Chem Phys 108:6109–6116
50. Delano WL, Lam JW (2005) Abstr Pap Am Chem Soc 230:1371–1372
51. Chou PY, Fasman GD (1978) Adv Enzymol Relat Areas Mol Biol 47:45–148
52. Jones DT (1999) J Mol Biol 292:195–202
53. Azevedo WF, Canduri F, Dos Santos DM, Silva RG, Oliveira JS, Carvalho LPS, Basso LA, Mendes MA, Palma MS, Santos DS (2003) Biochem Biophys Res Commun 308:545–552
54. De Azevedo Jr. WF (2008) Curr Drug Targets 9:1030–1030
55. De Azevedo Jr. WF, Dias R (2008) Curr Drug Targets 9:1031–1039
56. Dias R, De Azevedo Jr. WF (2008) Curr Drug Targets 9:1040–1047
57. Canduri F, De Azevedo Jr. WF (2008) Curr Drug Targets 9:1048–1053
58. Pauli I, Timmers LFSM, Caceres RA, Soares MBP, De Azevedo Jr. WF (2008) Curr Drug Targets 9:1054–1061
59. Dias R, Timmers LFSM, Caceres RA, De Azevedo Jr. WF (2008) Curr Drug Targets 9:1062–1070
60. De Azevedo Jr. WF, Dias R (2008) Curr Drug Targets 9:1071–1076
61. Caceres RA, Pauli I, Timmers LFSM, De Azevedo Jr. WF (2008) Curr Drug Targets 9:1077–1083
62. Barcellos GB, Pauli I, Caceres RA, Timmers LFSM, Dias R, De Azevedo Jr. WF (2008) Curr. Drug Targets 9:1084–1091
63. Timmers LFS, Pauli I, Caceres RA De Azevedo Jr. WF (2008) Curr. Drug Targets 9:1092–1099
64. Alexander CS, Yan X, Pei T (2005) Biophys J 88:1009–1017